Annihilation and reflection of spiral waves at a boundary for the Beeler-Reuter model

Daniel Olmos* and Bernie D. Shizgal†

Institute of Applied Mathematics, University of British Columbia, Vancouver, British Columbia, Canada V6T 1Z1

(Received 9 August 2007; revised manuscript received 19 December 2007; published 21 March 2008)

We employ a reaction diffusion equation with local dynamics specified by the Beeler-Reuter model to study the meandering of spiral waves. With the appropriate choice for the conductances of sodium and calcium channels, the trajectory of the tip of a spiral wave lies on a straight line. The phenomenon of annihilation or reflection of a spiral at the boundaries of the domain is studied. This phenomenon is analyzed in terms of the variable j, which controls the reactivation of the sodium channel in the Beeler-Reuter model. The results presented can have potential applications in the study of cardiac arrhythmias by providing insight on the interaction between spiral waves and obstacles in the heart.

DOI: 10.1103/PhysRevE.77.031918 PACS number(s): 87.19.Hh, 82.40.Ck, 87.16.A−

I. INTRODUCTION

An understanding of the propagation of waves in excitable media is a very important research area [1–4]. Particular attention has been given to the study of spiral waves [1,4–7]. A spiral wave is a self-sustained wave that rotates freely or around some obstacle. In cardiology, it is thought that spiral waves, which have been observed experimentally in isolated cardiac tissue [8,9], play an important role in cardiac arrhythmius. A very important feature of spiral waves is the motion of its tip [1,10]. For a particular set of parameters characterizing the medium, the spiral tip executes different trajectories which can be circular or more complicated patterns [7,11,12]. This phenomena, referred to as spiral meandering or compound rotation, was first noted by Winfree [13] and has been studied with different kinetic models [1,5,7,14]. The classic Fitzhugh-Nagumo (FHN) equation is a frequently chosen model [7,11,15]. When meandering occurs, the trajectory of the tip executes a flowerlike pattern [7,11], where the petals lie on a circle of radius R. When the petals lie outside the circle, the trajectory resembles a curve called a hypotrochoid, whereas when the petals lie inside the circle, the trajectory resembles an epitrochoid. By considering different parameter values in a particular model with excitable kinetics [5,11], it is possible to take the limit $R \to \infty$. In this case, which we refer to as the limiting R_∞ case with $R \gg 1$, the flower has almost an infinite radius, and the petals lie essentially on a straight line. A second feature of the spiral tip, called spiral wave drift, is the response of the spiral wave to an external perturbation [16–18]. In the present work we consider the effects of a boundary on the trajectory of the tip of a spiral.

Spiral drift due to boundary effects has been considered previously. It has been found experimentally [17] and studied numerically [15,18,19]. Gómez-Gesteira *et al.* [17] considered the Belousov-Zhabotinsky reaction and found that the boundary affected the trajectory of the spiral tip. The trajectory moved along the boundary, whereas in other cases the spiral was annihilated at the boundary [17]. Yermakova and Pertsov [18] analyzed the effects of the boundary on the trajectory of the spiral tip that followed a circular path. By considering no flux boundary conditions, they showed that the period of the spiral increases when the core of the spiral is close to the boundary. They also showed that the center of the circular trajectory drifted at constant speed along the boundary giving as a result a trajectory resembling the shape of a trochoid. However, the case when the trajectory of the spiral tip meanders and traces a more complex pattern other than a circle has not been considered. Osipov *et al.* [15] studied a discrete excitable model based on FHN dynamics with modifications to the medium properties and free boundary conditions. They observed annihilation and reflection of the spiral wave at the boundary [15]. Nikolaev *et al.* [19] considered a FHN-type model on a circular domain and studied the boundary effects on the tip trajectory for spiral waves subjected to an external periodic perturbation [19]. Finally, analytical studies about the interaction of a spiral wave with a boundary was presented by Aranson *et al.* [20] using a Fitzhugh-Nagumo-type equation.

In the present paper, we consider the Beeler-Reuter (BR) model [21] and study numerically the meandering of a spiral wave and the boundary effects on the motion of the tip trajectory. The BR ionic model is the simplest ionic model that reproduces the action potential of myocardial tissue and is widely used to model ventricular cells [5,22–24]. A detailed discussion of the BR model and comparisons with other ionic models have been presented elsewhere [25–27]. We also carry out a detailed comparison of our simulations with the BR and FHN models. In the simulations, we use no flux boundary conditions and observe annihilation or reflection due to the interaction of the spiral wave with a boundary. Experiments in isolated cardiac tissue [8,9,28,29] have been carried out to study the interaction of spiral waves with obstacles and the boundaries of the tissue. Davidenko *et al.* [8], Pertsov *et al.* [9], and Ikeda *et al.* [28] showed experimentally annihilation of spiral waves at the boundary. Also, Ikeda *et al.* [29] observed attachment of meandering spirals to an obstacle of some minimum size. Therefore, the phenomena of annihilation and reflection observed in the computer simulations in the present paper suggest that spiral-boundary and

*daniel@iam.ubc.ca

†Present address: Department of Chemistry, University of British Columbia, 2036 Main Mall, Vancouver, British Columbia, V6T 1Z1; shizgal@theory.chem.ubc.ca; URL: http://www.chem.ubc.ca/personnel/faculty/shizgal/

spiral-obstacle interactions do not necessarily end in annihilation at a boundary or attachment to an obstacle as observed experimentally.

When the spiral meanders and is close to the boundary (with no flux boundary conditions), it is observed that the trajectory can be annihilated or reflected at the boundary. In the case where the trajectory is reflected, the angle of reflection is not necessarily equal to the angle of incidence. Therefore, the main question we address here is to find the conditions for which the spiral is annihilated at the boundary. In order to analyze the effects of the boundary on a meandering spiral, we focus attention on the degenerate R_∞ limiting case.

The infinite radius regime is just a transition from the outward petal to the inward petal flower tip trajectory and therefore is not a generic behavior [11]. The analysis of the R_∞ case is considered due to its simplicity compared to the case of finite R. Near the boundary, the behavior of the tip of a spiral can be approximated by the R_∞ case and the results obtained for this limit may also provide an understanding for the case when R is finite.

In Sec. II, we present the model equations used in the numerical experiments and we also provide a description of the numerical method employed in their solution. In Sec. III, we present the results of numerical simulations for different values of R, including the R_∞ case. Some of the boundary effects observed in compound rotation are shown for the R_∞ case in Sec. IV. In Sec. V, we present the phenomenon of annihilation at a boundary as a function of the incident angle of the trajectory obtained with the R_∞ case. In Sec. VI, an argument based on the reactivation variable j for the sodium channels is discussed to explain the phenomenon of annihilation and reflection of a spiral at a boundary. Due to the complexity of the problem, we present a qualitative rationalization to explain why the probability of annihilation varies with respect to the incident angle of the trajectory for the R_∞ case (Sec. VII). Results with the FHN equations are presented in Sec. VII A. Finally, we present a summary of the results and conclusions in Sec. VIII.

II. MEMBRANE MODELS AND NUMERICAL METHODS

Spiral wave dynamics in excitable media, particularly trajectories of the spiral tip, have been extensively studied with reaction diffusion partial differential equations [1,5,7] as well as reduced ordinary differential equation models [11,30]. The simplest model used is based on the Fitzhugh-Nagumo equations which have been discussed by different authors [7,27,31,32].

In this work we considered the BR kinetic model [21], which has more realistic dynamics than the FHN equations. The BR model, which is based on the Hodgkin-Huxley formalism, consists of a set of eight coupled nonlinear ordinary differential equations described in [21]. The transmembrane potential V satisfies the equation

$$\frac{dV}{dt} = -\frac{1}{C_m}(I_{ion} - I_{app}), \tag{1}$$

where C_m is the membrane capacitance, I_{app} is a stimulus current, and I_{ion} corresponds to the sum of four ionic currents I_{k_1}, I_{x_1}, I_{Na}, and I_{Ca} where their form is given by Eqs. (A1)–(A4) in Appendix A. I_{Na} is the fast inward current and is carried by sodium ions, whereas I_{Ca} is the slow inward current and is carried by calcium ions. I_{Na} and I_{Ca} are voltage and time dependent currents. I_{k_1}, I_{x_1} are the time independent and time dependent outward currents, respectively, carried mostly by potassium ions. I_{x_1}, I_{Na}, and I_{Ca} are controlled by gate variables. Each of the six gate variables satisfies the relationship given by Eq. (A6) in Appendix A. The BR model also contains the equation that controls the intracellular calcium concentration of the cell and is given by Eq. (A5). The BR model is extended to spatiotemporal dynamics by adding a diffusion term in the membrane potential equation [Eq. (1)] giving

$$\frac{\partial V}{\partial t} = D\nabla^2 V - \frac{1}{C_m}(I_{ion} - I_{app}), \tag{2}$$

where $D=\sigma/S_v C_m$ is the diffusion coefficient for the isotropic case where σ refers to the conductivity of the medium and S_v is the ratio of cell surface area per unit of volume [27,33]. For this work the values of D and C_m are $0.1\ \mathrm{mm^2\ m\ s^{-1}}$ and $1\ \mu\mathrm{F\ cm^{-2}}$, respectively [1,5]. The present calculations were carried out over a square domain $\Omega=[-L,L]\times[-L,L]$. The reaction diffusion equation, Eq. (1), is solved on this domain with zero flux boundary conditions.

The numerical method used in this work is a variation of the method considered by Yang and Shizgal [34] and in a paper to be published [35]. In each dimension, the domain was divided into N_i overlapping subdomains of the same length. Each subdomain has N_{ch} Chebyshev-Lobatto collocation points [34,35]. Each subdomain has two points in common with the neighboring subdomains so that the total number of collocation points is $N=(N_{ch}-1)N_i+2$. Due to the multiple spatial and temporal scales in the BR model, we consider an operating splitting method [36–38] to separate the diffusion from the reactive processes. For spatial discretization, which is considered in the diffusion process, we used a nonuniform grid as defined with a multidomain method based on Chebyshev collocation points [35,39]. In order to solve the BR equations, we considered a procedure similar to the operator splitting algorithm presented by Qu and Garfinkel [37] with some minor differences. The calculations for the reaction part were speeded up by dividing the domain Ω into smaller squares Π of size 30 points in each dimension. In each square Π, we calculated the values $|\partial^2 V/\partial x^2|$ and $|\partial^2 V/\partial y^2|$ and as soon as either of these values were larger than 5 at some point $(x^*,y^*)\in\Pi$, we defined the whole square as a place where the front might be located. In the same way, all the eight squared neighbors of Π were considered in the same way as the region Π to assure correct propagation of the wave front. We finally obtain two main regions, one where the fast changes in time and space occur and one with no fast changes. In the region where V changes very slowly (second derivatives less than 5), we solve the dynamics as in [37]. Because V changes slowly, we consider V as constant for a time step and solve Eq. (A6) for V with respect to time analytically, by taking $\bar{Y}_i$ and τ_i constant for

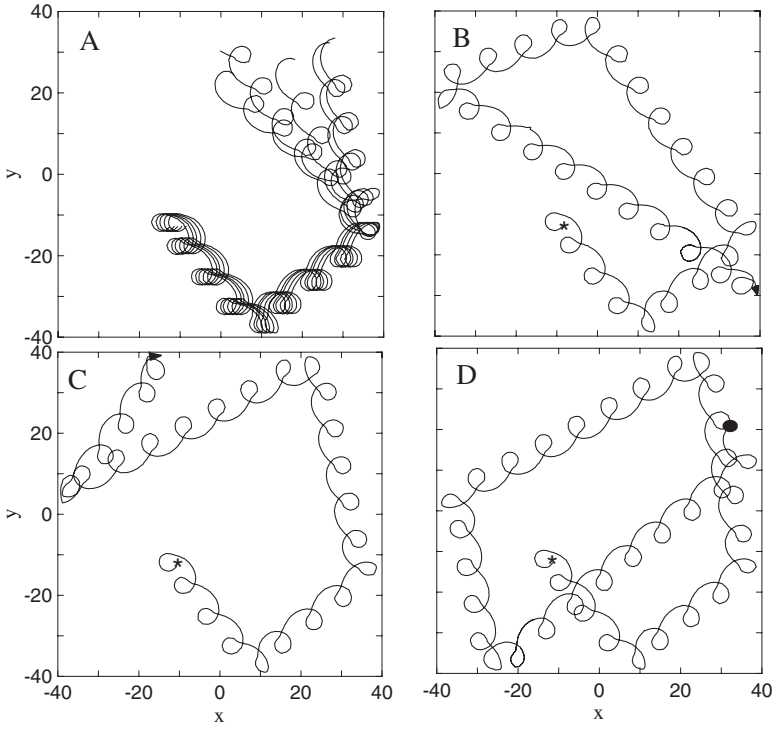

FIG. 1. Spiral tip trajectories with the BR model with $g_{\mathrm{Na}}=2.38$ mS cm^{-2} and $g_S=0.03$ mS cm^{-2} for the limiting R_∞ case. (A) Five tip trajectories. Each trajectory is a small horizontal translation of the others. [(B) and (D)] The same trajectories as in (A) but for a longer integration time. The initial point of each trajectory is marked with (*) and the end with (●). The filled arrow indicates the place at which the trajectory leaves the domain; x and y are in mm; $N=452$ points in each dimension.

that interval of time. In order to calculate the α's and β's in Eqs. (A7) and (A8), we proceed as in [5] where tabulated values given by step function approximations of $\alpha(V)$ and $\beta(V)$ as a function of V are considered. In Π, the region where fast changes of V occur, we solve Eq. (A6) numerically with an explicit second order Runge-Kutta scheme with a time step $\Delta t=0.01$, four times smaller than in the region with no fast changes. For the multidomain approach used in this work [35,39], we choose $N_i=150$ and $N_i=180$ subintervals with $N_{ch}=5$ points per subinterval, giving a total of $N=452$ and $N=542$ points in each dimension, respectively. The size of the domain is $2L\times 2L$ with $L=40$ mm. Convergence to the solution for the one dimensional problem was obtained with $N=752$ points. We chose $N=452$ for simulations carried out for long time whereas $N=542$ was chosen to improve accuracy for short time integrations. The computations were carried on a Beowulf cluster using a single processor with an internal clock speed of 3.06 GHz. The computational time for the simulations considered in this work is calculated for the time that a spiral traces a complete rotation. When $N=452$, as considered for the computations in Sec. III, a complete rotation takes about two hours to compute and represents about 110 ms of simulation time. For $N=542$, used in Sec. IV and after, the same calculation takes almost four hours to compute.

III. NUMERICAL RESULTS

Following the work by Efimov *et al.* [5], we set the calcium conductance to $g_S=0.03$ mS cm^{-2} and varied g_{Na} over a range of values. We focus attention on the parameter value $g_{\mathrm{Na}}=2.38$ mS cm^{-2} which give the R_∞ case. With these parameters, the tip of the spiral wave meanders such that the petals lie on a straight line. Even when the petals appear to lie on a straight line, it is not possible to be certain that the R_∞ has been achieved. For practical purposes $R\gg 1$ will be considered as the R_∞ case. In Fig. 1(A), five trajectories are shown for different initial conditions for an integration time of $t^*\approx 1.75$ s. The initial conditions were constructed following the procedure given in Appendix B with $t_g=50$ ms, $c_1=30$, $c_2=25$, $\alpha=0$ and varying the parameter y_0 from -10 mm to -14 mm with increments of 1 mm. As a result, the different initial conditions are a copy of each other translated horizontally by a distance of approximately 0.8 mm. In Fig. 1(A), all the trajectories hit the boundary and get reflected with the same angle for the first reflection but not the second. This behavior is due to the fact that each trajectory is a horizontal translation of the other. Therefore, the distance from the initial position of the tip trajectory to the boundary is exactly the same for all five trajectories. The time required for all the trajectories to hit the boundary for the first time is $t=0.596$ s. However, when the trajectories hit the boundary a second time [Fig. 1(A)], the angles of reflection of each trajectory are different. Each trajectory has to travel a different distance from each other before hitting the boundary a second time. The corresponding times when the tip trajectories hit the boundary for the second time are $t^*=1.0326, 1.0376, 1.0426, 1.0476$, and 1.0526 s, respectively.

Three of the trajectories shown in Fig. 1(A) are shown in Figs. 1(B)–1(D) for longer integration times up to 5 s. The initial position of the trajectory is marked with an asterisk. It is clear that the solutions follow completely different paths after the second reflection from the boundary. Moreover, in Figs. 1(B) and 1(C) it is shown that the spiral tip annihilates instead of being reflected at the boundary as shown by the arrows at times $t\approx 3.62$ and 3.22 s, respectively, ending the spiral motion. By contrast, the trajectory shown in Fig. 1(D), which is shown for time up to $t\approx 4.3$, remains inside the

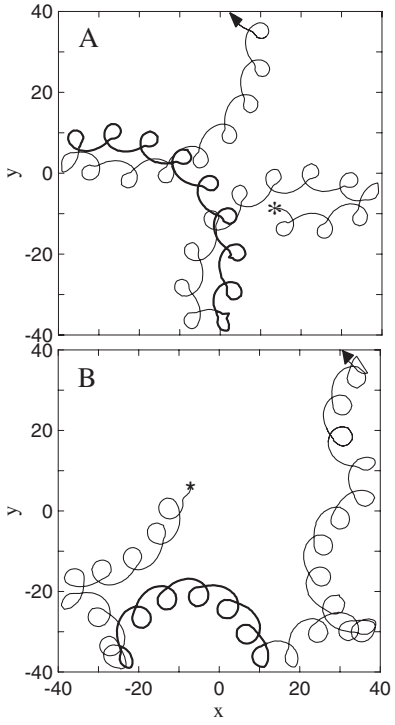

FIG. 2. Spiral tip trajectories with the BR model with $g_S=0.03$ mS cm^{-2} and (A) $g_{\mathrm{Na}}=2.41$ mS cm^{-2}; (B) $g_{\mathrm{Na}}=2.34$ mS cm^{-2}. The initial point of the trajectory is marked with (*) and the filled arrow indicates where the spiral gets annihilated. For (A) $y_0=10$ mm and $t_g=51.5$ ms and for (B) $y_0=-10$ mm and $t_g=85$ ms; x and y are in mm; $N=452$ points in each dimension.

domain even for times as large as 5 s. The spiral tip in Fig. 1(D) was followed until the point indicated by a solid circle. Notice also that in Figs. 1(B) and 1(C) the spiral tip hits the boundary 5 times in both cases before they annihilate at the boundary. The spiral tip in Fig. 1(D) gets reflected at the boundary 6 times and still remains in the domain.

The phenomenon of reflection and annihilation at the boundary also occurs for finite R, as shown in Fig. 2. In Fig. 2(A), an outward petal flower pattern with $R\approx 30$ mm is shown, whereas in Fig. 2(B) an inward petal flower with $R\approx 16$ mm occurs. The radius R in these trajectories, which start at the asterisk, was estimated from the semicircles shown in bold. In order to obtain such trajectories the parameters in Eq. (2) are $g_s=0.03$ mS cm^{-2} with $g_{\mathrm{Na}}=2.41$ mS cm^{-2} and $g_{\mathrm{Na}}=2.34$ mS cm^{-2} for Figs. 2(A) and 2(B), respectively. In both cases, the effect of reflection at the boundary is observed until the fourth and the sixth time the tip of the spiral hits the boundary where annihilation occurs.

IV. BOUNDARY EFFECTS ON THE ROTATION PERIOD IN COMPOUND ROTATION

The study of compound rotation is much more complex than simple rotation. For simple rotation, when the system has no external perturbations, a trajectory far from the boundary remains circular. However, when such a trajectory is close enough to the boundary, drift occurs [18] and the trajectory changes from a circle to a curve called a trochoid. Annihilation of the spiral wave when its tip trajectory is circular occurs when the tip trajectory is too close to the boundary as described in [40]. Another phenomenon observed in [18] is that the rotation period decreases when the distance of the center of the circular trajectory to the boundary is decreased.

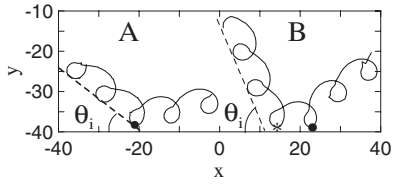

FIG. 3. The dashed line indicates the line on which the petals of the tip trajectory lie and θ_i is the incident angle. (A) The filled circle is the place where the tip hits the boundary. (B) A special case of reflection at the boundary. There are two points where a minimum with the boundary is reached (asterisk and filled circle). The filled circle point is the one considered to be the point at which the tip hits the boundary; $g_{\mathrm{Na}}=2.37$ mS cm^{-2}, $g_S=0.03$ mS cm^{-2}; x and y are in mm.

We focus on the R_∞ case to study the annihilation-reflection phenomenon for compound rotation. By considering the R_∞ case we remove the variable R as a parameter, avoiding the possible complicated behaviors shown in Fig. 2(B). Also, the trajectories obtained with the R_∞ case can be seen as a local linear approximation of a trajectory with finite R when the spiral tip is about to interact with the boundary. Therefore, studies with the R_∞ case will provide information about the annihilation-reflection properties for R finite. For this analysis, we solve the standard BR equations [5] with $g_{\mathrm{Na}}=2.37$ mS cm^{-2} and $g_S=0.03$ mS cm^{-2}. With these parameters we obtain a trajectory of the tip with $R\gg 1$, which is considered to be in the R_∞ case.

Figure 3 shows the reflections of two linear spiral tip trajectories from a boundary with different angles of incidence θ_i defined by the dashed line which is tangent to the petals of each trajectory. For the R_∞ case, we consider that the trajectory tip has reflected from the boundary when there is a change in the direction of the line on which the petals lie and this direction is maintained for two or more spiral rotations. The tip is considered to hit the boundary at the first point along the trajectory that reaches a minimum distance with the boundary [filled circle in Fig. 3(A)]. A different type of reflection is shown in Fig. 3(B), where there are two positions along the tip trajectory at which the minimum is reached (asterisk and filled circle). In this case, we consider the second point (filled circle) as the place where the tip hits the boundary. The angle of incidence θ_i plays an important role in later discussions of reflection and annihilation of spiral waves at a boundary.

Figure 4(A) shows one rotation of the spiral wave and the tip trajectory starting from the solid circle (a) to the arrow. This curve defines a unit of trajectory and consists of a petal and an arc. The petal is the part with large curvature given by the small loop whereas an arc is the part of the unit with small curvature. The points marked a–d on the unit trajectory are discussed in Sec. VI. The period of rotation for the cho-

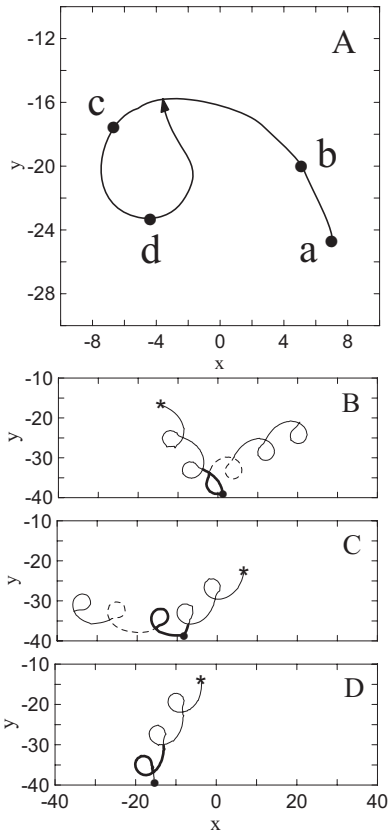

FIG. 4. (A) A spiral tip trajectory unit far from the boundary. It consists of a petal and an arc. Parameters as in Fig. 3. Spiral tip trajectories for incident angles equal to (B) $\theta_i=60°$, (C) 140°, and (D) 120°. The filled circle [(B)–(D)] indicates the place where the tip hits the boundary. For (A) the range of values of the j variable ahead of the propagating front next to the spiral tip, when one spiral cycle unit is traced (a) $j\in[0.78,0.84]$, (b) $j\in[0.84,0.9]$, (c) $j\in[0.9,0.95]$, and (d) $j\in[0.95,0.99]$; x and y are in mm.

sen parameters is $\tau_0=120$ ms and the arc length of the unit of trajectory is $L_0=24.8$ mm. The trajectories are thus taken to be made up of consecutive unit trajectories. However, close to the boundary, the shape, length, and period of rotation of a unit of trajectory are not the same as for those units far from the boundary as shown in Figs. 4(B)–4(D). Figure 4(B) is for $\theta_i=60°$ and the unit of trajectory starting from the asterisk, is conserved for the first two rotations of the spiral. The shape is changed for the third unit of trajectory (bold) owing to the reflection from the boundary. The unit of trajectory after reflection is shown with the dashed line in Fig. 4(B). A similar behavior is observed in Fig. 4(C) for $\theta_i=140°$. In Fig. 4(D) with $\theta_i=120°$, the trajectory disappears at the boundary.

The first row of Table I gives the period of rotation τ_0 and the arc length L_0 for the first two units of trajectory [starting from the asterisk in Figs. 4(B)–4(D)], which are far from the boundary. These parameters for the units of trajectory shown in bold and a dashed line in Figs. 4(B) and 4(D) are reduced from their values far from the boundary (second and third rows in Table I). The opposite effect is observed in Fig. 4(C), where τ_0 and L_0 for the units of trajectory in bold and a dashed line have increased relative to the first two units far from the boundary (Table I). For Fig. 4(D) there is no dashed unit as the tip trajectory disappears at the boundary. The results in Fig. 4 and Table I illustrate the complexity of the interaction of spiral waves with a boundary in terms of the morphology of trajectory units.

TABLE I. The total length L_0 in millimeters, and period of rotation τ_0 in milliseconds of a unit of trajectory for three cases shown in Figs. 4(B)–4(D). Notice that for case D corresponding to Fig. 4(D) as the trajectory was annihilated at the boundary.

	B		C		D	
	L_0	τ_0	L_0	τ_0	L_0	τ_0
First two	24.8	120	24.8	120	24.8	120
Bold	16.5	78	25.2	121.7	22.5	108.7
Dashed	22.4	110.4	26.6	133.14		

V. ANNIHILATION AND REFLECTION AS A FUNCTION OF THE INCIDENT ANGLE

In order to understand the factors that determine annihilation and reflection of spiral waves, we consider a fixed angle θ_i with different initial conditions. A spiral tip trajectory with a specific incident angle θ_i can be constructed as described in Appendix B. For the results that follow, we take $g_{\mathrm{Na}}=2.37$ mS cm^{-2} and $g_S=0.03$ mS cm^{-2}, which we take as the R_∞ case. In order to obtain a trajectory with incident angle $\theta_i=120°$, we choose initial conditions such that $y_0=0$, $c_1=75$, $c_2=72$, and $\alpha=1.53$. With this initial condition, we find by trial and error the linear trajectories shown in Fig. 5(A), with $t_g=105$ ms and $t_g=150$ ms, which have the same θ_i. In both cases the spiral tip disappears at the boundary. The tip trajectories in Figs. 5 and 6 were constructed in this way such that $\theta_i=120°$ and $\theta_i=70°$, respectively.

The trajectory on the right in Fig. 5(A) is a horizontal translation of the one at the left but with an extra petal. The extra petal is due to the different values of t_g for each of the two trajectories. With $t_g=150$ ms, the initial position (asterisk) of the tip trajectory is farther from the lower boundary by a distance $\lambda_v=8.78$ mm, than the initial position (asterisk) of the tip trajectory, with $t_g=105$ ms. The quantity λ_v gives the distance traveled by the tip in the vertical direction during a complete rotation of the spiral wave. As a consequence, an extra petal is observed for the trajectory on the right. Since $\lambda_v=\lambda\sin\theta_i$, the wavelength λ is the distance between two petals that are far from the boundary. If a third tip trajectory is generated with the same θ_i but with the initial position of the tip $2\lambda_v$ mm farther from the lower boundary than the initial position of the tip trajectory with $t_g=105$ ms, this new trajectory will have two extra petals compared to the trajectory obtained with $t_g=105$ ms. This third trajectory is found with $t_g=195$ ms, and there is an apparent periodicity in t_g of 45 ms.

Two trajectories with initial positions separated by a vertical distance λ_v such as in Fig. 5(A) exhibit the same behavior when the corresponding spirals hit the boundary. Therefore, the outcome of a spiral wave hitting the boundary is a

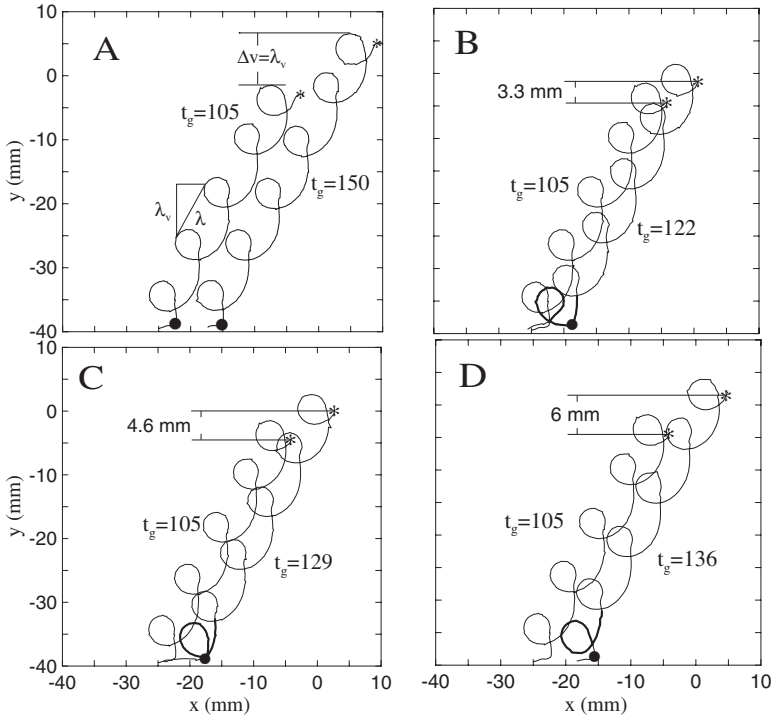

FIG. 5. Spiral tip trajectories for $\theta_i=120°$, and different values of t_g. (A) $t_g=105$ (left) and $t_g=150$ (right). [(B)–(D)] Tip trajectories with $t_g=105$ ms (left) and $t_g=122,129$, and 136 ms, respectively. The filled circle in each plot indicates the position along the trajectory where the tip hits the boundary. Parameters as in Fig. 3.

periodic function of the distance of the initial position of its tip trajectory with respect to the boundary, and the period is λ_v. In order to obtain trajectories such that the initial position of their tip trajectory lie within the period λ_v, we take values of $t_g \in [105,150]$. Different values of t_g inside this interval will give trajectories whose initial distance from the boundary is different from each other. The distance of the initial positions of the trajectories with $t_g=105$ and $t_g=150$ from the boundary, will differ exactly by $\lambda_v=8.8$ mm. Therefore, all the possible cases by which a spiral wave can hit the boundary for $\theta_i=120°$, can be obtained by taking $t_g \in [105,150]$. We thus study the phenomenon of reflection and annihilation by choosing values of t_g in the interval $t_g \in [105,150]$ and follow the fate of each spiral.

In Figs. 5(B)–5(D), we show a limited number of tip trajectories for spirals calculated with $t_g=122,129$, and 136 ms, respectively. In Figs. 5(B)–5(D), the initial positions (asterisks) of the trajectories with $t_g=122,129$, and 136 ms, are farther from the boundary by 3.3, 4.6, and 6 mm, respectively, than is the initial position (asterisk) of the tip trajectory with $t_g=105$ ms that is also shown for comparison. These trajectories annihilate at the boundary.

With $t_g=105$ ms, the tip trajectory changes its direction abruptly and then disappears at the boundary [Fig. 5(A)]. When t_g is increased to 122 ms [Fig. 5(B)], the trajectory does not disappear at the boundary immediately but a new petal, shown in bold, is formed first. With a further increase in t_g, this new petal gets closer to where the trajectory hits the boundary. From Fig. 5(C), the new petal moves until it appears before the tip hits the boundary. In frame (D), a new spiral unit (bold) has been formed. The new spiral unit is completely formed when $t_g=150$ ms [Fig. 5(A)], as expected from the definition of λ_v. The phenomenon of the creation of a new petal repeats as we increase further the value of t_g above 150 ms. A new petal will be completely formed when $t_g=195$ ms, which gives a trajectory that starts $\lambda_v=8.8$ mm farther from the boundary than the trajectory obtained with $t_g=150$ ms.

We show complementary results for $\theta_i=70°$ in Fig. 6. The trajectories were generated with the procedure in Appendix B, with $y_0=-20$ mm, $c_1=35$, $c_2=33$, $\alpha=0.123$ such that $\theta_i=70°$. Following the same procedure as for $\theta_i=120°$, we find in this case by trial and error two tip trajectories given by the values $t_g=44$ and $t_g=71$ [Fig. 6(A)]. Analogous to the case with $\theta_i=120°$, the trajectory at the right in Fig. 6(A) is a horizontal translation of the one at the left but with an extra petal. In this case, the initial position (asterisk) of the tip trajectory with $t_g=71$ ms is $\lambda_v=8.9$ mm farther from the bottom boundary than is the initial position (asterisk) of the trajectory with $t_g=44$ ms. Following the same reasoning as in the previous example ($\theta_i=120°$), we take representative values of $t_g \in [44,71]$. In Figs. 6(B)–6(D), we show three trajectories with intermediate values of t_g equal to 52,60, and 67 ms, respectively. These three trajectories have the initial position (asterisk) of their trajectories, 2.7, 5.4, and 7.8 mm farther from the boundary compared to the initial position of the trajectory given by $t_g=44$.

In Fig. 6(A), where $t_g=44$ ms, the tip hits the boundary and the spiral disappears. However, when t_g is increased to 52 ms [Fig. 6(B)], the spiral wave gets reflected at the boundary. Therefore, annihilation and reflection of the spiral wave is observed with the same angle θ_i. In Figs. 6(B)–6(D), the different responses of the tip trajectory at the boundary as we change the value of t_g are shown. For $t_g=71$ ms [Fig. 6(A)], the distance from the initial position of the trajectory to the boundary is farther $\lambda_v=8.9$ mm than the same distance for the trajectory with $t_g=44$ ms. Therefore, the response of the trajectories with $t_g=44$ and $t_g=71$ ms is the same. In-

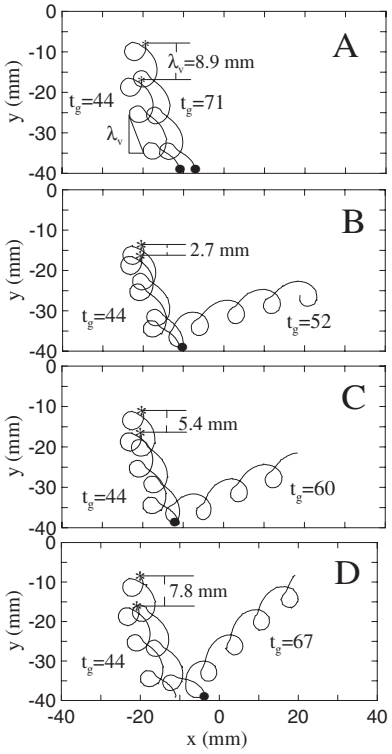

FIG. 6. Spiral tip trajectories for $\theta_i=70°$, and different values of t_g. (A) Tip trajectories with $t_g=44$ (left) and $t_g=71$ ms (right). [(B)–(D)] Tip trajectories with $t_g=44$ ms (left) and $t_g=52,60$, and 67 ms, respectively. The filled circle in each plot indicates the position along the trajectory where the tip hits the boundary. Parameters as in Fig. 3.

creasing the value of t_g beyond 71 ms will repeat the observed behavior in Figs. 6(B)–6(D), which illustrates the periodicity with period 27 ms.

Annihilation of the spiral wave with $\theta_i=120°$, shown in Fig. 5 and annihilation and reflection of the spiral with $\theta_i=70°$ shown in Fig. 6 for different values of t_g, raises the question as to which angles θ_i is annihilation observed. Moreover, are there particular values of θ_i that are more favorable for annihilation to occur than others? Are there values θ_i where annihilation does not occur? In Fig. 7, we show the fraction $F_A(\theta_i)$ of the spirals that are annihilated at the boundary as a function of the incident angle θ_i. In this graph, we considered the range of angles from 20° to 160° in steps of 10°. For each angle θ_i, we have shown that there exists a pair of parallel tip trajectories with values t_g^1 and t_g^2 such that the difference in the initial positions of the two trajectories is the distance $\lambda_v=\lambda \sin \theta_i$ mm from the boundary. Therefore, we sample 40–60 tip trajectories for each angle θ_i with equidistant values of t_g between $t_g \in [t_g^1, t_g^2]$. In Fig. 7, we show that for $\theta_i \in [20,50]$ and $\theta_i \in [150,160]$, every spiral wave is reflected at the boundary. There is thus a range of values $\theta_i \in (50,150)$, for which at least one spiral wave is absorbed at the boundary. For $\theta_i=120°$, we find that all the trajectories considered are absorbed by the boundary.

In order to understand the mechanisms that influence the annihilation and reflection of the spirals, it is necessary to understand the physical mechanisms occurring near the tip of

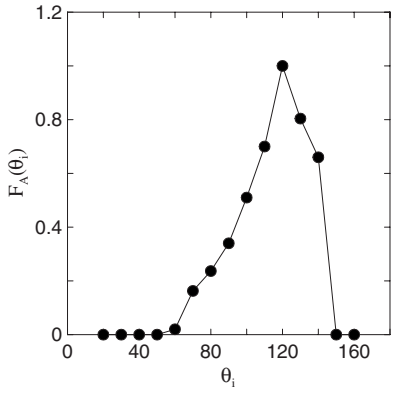

FIG. 7. Fraction of the trajectories, $F_A(\theta_i)$, that were annihilated by the boundary as a function of the incidence angle θ_i.

the spiral during the trace of a unit of trajectory. In the next section, we present a study of the propagation of a wave break to understand the shape of a spiral tip trajectory; the same study will be helpful to understand why we obtain annihilation and reflection of a spiral at a boundary. A rationalization of the results presented in Fig. 7 is considered in Sec. VII after discussing the physical mechanisms involved in annihilation and reflections of spiral waves at a boundary.

VI. ROLE OF EXCITABILITY IN CONTROLLING REFLECTION AND ANNIHILATION AT THE BOUNDARY

The reflection and annihilation of spiral waves at a boundary can be explained by considering the gate variable $j \in [0,1]$ in the BR equations (Appendix A). The variable j in the BR model controls the reactivation of the sodium channels, responsible for the initiation of an action potential (AP) [21]. The term m^3hj controls the opening and closing of the sodium gate, where at rest $m \approx 0$, $h \approx 1$, and $j \approx 1$. At the beginning of the AP, m approaches 1 on a very fast time scale while h and j remain near 1, such that $m^3hj \approx 1$. At this time, the $\bar{g}_{\mathrm{Na}}=g_{\mathrm{Na}}m^3hj$ conductance is maximized, giving a large influx of sodium ions which depolarizes the cell. However, after a few milliseconds, the inactivation variable h and the reactivation variable j approach zero, so that $m^3hj \approx 0$, and then the sodium conductance $\bar{g}_{\mathrm{Na}} \approx 0$, terminating the depolarizing current. Another excitation is prevented until the parameters h and j get close enough to 1. The reactivation parameter j sets the time when the medium is ready to accept another AP. This suggests that when the tip of a spiral hits the boundary, the spiral wave will be annihilated if the gate variable has not sufficiently recovered at regions near to the tip of the spiral wave so as to accept an AP.

In order to clarify this assertion, we present an analysis of the propagation of an AP in one dimension and the response to an external stimulus, following the study of Glass and Josephson [41] for the propagation of a pulse on a ring. In Fig. 8(A), we show the propagation of a one-dimensional (1D) AP from left to right, where V (solid line) and j (dashed line) are plotted versus x. In this case, the initial propagating pulse is generated by applying a stimulus current, I_{app}, as given in Eq. (B1), with $c_1=100$, $c_2=95$, and $\alpha=0$ for the first

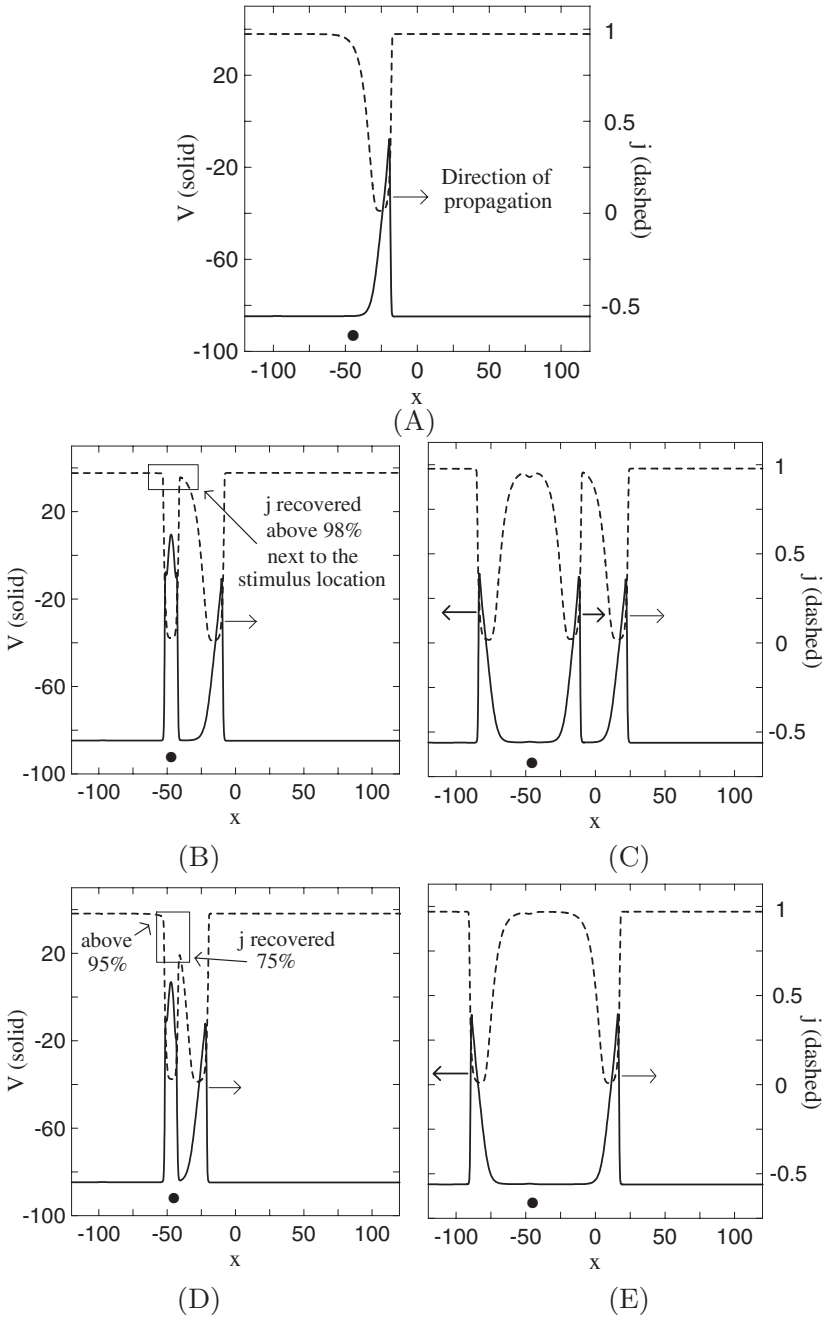

FIG. 8. (A) Propagating pulse for the BR model in 1D. $g_s=0.03$, $g_{Na}=2.37$ mS cm^{-2}. V (solid) and j (dashed) are plotted versus x at a fixed time. A stimulus is applied at $x=-47.5$ mm (●) at times (B) $t^*=280$ and (D) $t^*=240$ ms. (B) The gate variable j is above 98% recovered at the position at which the stimulus is applied. (C) Response of the stimulus applied at $t^*=280$. Two new single pulses are generated (bold arrows). (D) The gate variable j has recovered 75–85 %. (E) Only one AP was generated with the stimulus (bold arrow). The propagation of the new AP in the direction of the original pulse was blocked as j has not recovered completely; x and y are in mm.

millisecond. We apply a second stimulus for 1 ms at $x_0=-47.5$ (filled circle) after the first propagating pulse has passed the location $x_0=-47.5$.

The results of applying the stimulus at $t^*=280$ ms and $t^*=240$ ms are summarized in Figs. 8(B)–8(E), respectively. The stimulus also has the form of Eq. (B1) with $c_1=50$, $c_2=45$, and $\alpha=0$. In Figs. 8(B) and 8(D), we show the plot of V and j after the stimulus has been applied, at times $t^*=280$ ms and $t^*=240$ ms, respectively. In both cases [Figs. 8(B) and 8(D)], the variable V attains a maximum and j attains a minimum at x_0 as a result of the stimulation. For the case $t^*=280$ [Fig. 8(B)], the stimulation occurred when j is more than 98% recovered as shown by the value of j inside the small box [Fig. 8(B)] close to x_0. Due to the high recovery level of the j gate close to the point where the stimulus is applied, two new APs are generated symmetric about x_0 [Fig. 8(C)], one that propagates in the direction of the original AP and a second one going in the opposite direction, as indicated by the bold arrows in Fig. 8(C) at a later time. A different result is obtained when the stimulus is applied at $t^*=240$ ms [Fig. 8(D)]. From Fig. 8(D), the stimulation occurred when the j variable is recovered within the range 75–95%, as shown by the values of j inside the small box [Fig. 8(D)] next to x_0. In this case, one AP in the opposite direction to the original pulse is generated, as indicated by the bold arrow in Fig. 8(E) some subsequent time. However, an AP could not be generated in the same direction as the original pulse [Fig. 8(E)]. The reason is that at the region on the left of x_0, j is recovered above 95% and an AP propagates, whereas on the right of the location stimulus, the gate

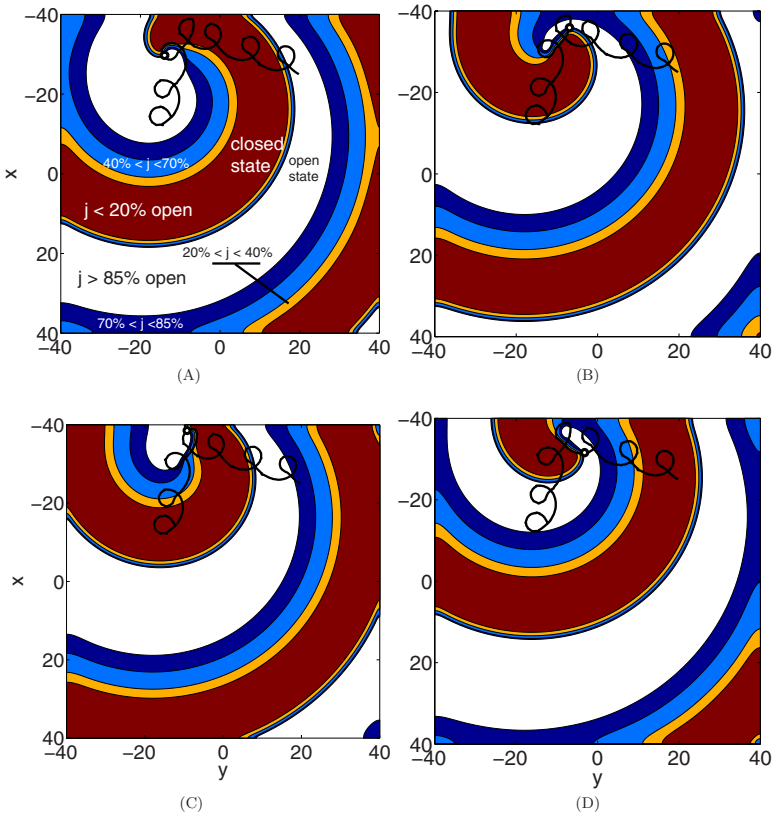

FIG. 9. (Color online) Reflection of a spiral for $\theta_i=80$, $t_g=68$ ms. The contour plots that are shown for different integration times represent different stages of recovery of the j variable. The black dot filled in white is the location of the tip of the spiral for that specific time; x and y are in mm.

j is less than 75% recovered, blocking the propagation of an AP.

The principle that an AP cannot be generated if j is not completely recovered is applied to the present study of reflection and annihilation of spiral waves at a boundary. Regions where the sodium channels are in the process of reactivation $(0 \leq j \leq 0.7)$, can be considered as regions of low excitability, whereas regions where the sodium channels are activated $(j > 0.96)$ can be considered as regions of high excitability. In Fig. 4(A), we have noted the increase in excitability along a unit of trajectory that increases from the arc portion (points a and b) to the petal portion (points c and d). We thus qualitatively relate the increase in excitability with an increase in the curvature of a unit of trajectory. It is important to distinguish between the curvature of the tip trajectory and the curvature of the spiral front as emphasized by Efimov *et al.* [5].

The complex dynamics of the interaction of a spiral wave with a boundary is shown for reflection in Fig. 9 and for annihilation in Fig. 10. Both graphs are for $\theta_i=80°$ with $t_g=68$ ms for Fig. 9 and 56 ms for Fig. 10. We show in these figures contour plots of the recovery variable j. The white region is where the j gate is at least 85% recovered and into which an action potential can propagate. The other colored areas denote different levels of the reactivation variable j where the widest colored area denotes a recovery of at most 20%, which means that the gate j is essentially closed. The narrower bands are intermediate levels of recovery as shown on the figures. The black dot filled in white denotes the location of the tip of the spiral.

The spiral tip trajectory in Fig. 9 starts at the point with coordinates $x \approx -14$ and $y \approx -11$ mm, and moves towards the upper boundary with $\theta_i=80°$. In Fig. 9(A), the tip of the spiral is located at a petal. It propagates into the white region which is at least 85% recovered. In Fig. 9(B), the tip gets very close to the boundary where it is located on the fourth petal shown which is deformed relative to the petals far from the boundary. The front propagates within a region that is highly excitable. However, the tip of the spiral cannot form a high curvature trajectory as in Fig. 9(A) due to the presence of the preceding propagating wave [5]. In Fig. 9(C), the tip of the spiral is at its closest approach to the boundary of the medium. The front next to the tip of the spiral continues to propagate as the region ahead of it is recovered and the spiral is reflected at the boundary as is shown in Fig. 9(D). In Fig. 9(C), when the region near the tip gets excited resulting in a deformation of the tip trajectory at the boundary, the front propagating in this region encounters the waveback [42] of the previous excitation of the spiral. The waveback is the fast transition in voltage that occurs during the repolarization of a propagating wave. The propagation of the new front near the tip in Fig. 9(D) is in a region of low excitability, characteristic of an arc of the unit of a trajectory. The front has reached the waveback of the preceding propagating wave and as a consequence, the angle of the line along which the petals lie is changed.

An example of spiral annihilation is shown in Fig. 10 for $\theta_i=80°$ and $t_g=56$ ms. In Fig. 10(A), the spiral tip is in a region that is not completely recovered and the tip of the spiral wave propagates into the white recovered region and the tip traces a curve with a large curvature, which is a petal. In Fig. 10(B), the tip of the spiral is very close to the boundary and is propagating in a region that is not recovered. The spiral wave is reflected as shown in Fig. 10(C) as the excit-

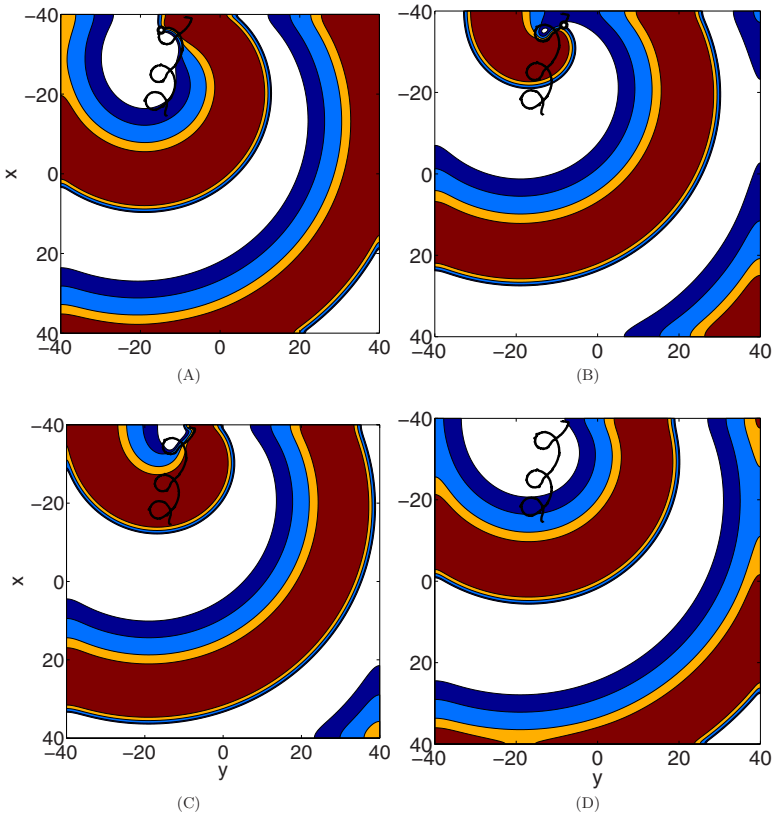

FIG. 10. (Color online) Annihilation of a spiral for $\theta_i=80$, $t_g=56$ ms; x and y are in mm. See the caption to Fig. 9.

ability is insufficient to cause recovery. In Fig. 10(D), the tip disappears at the boundary and the spiral wave motion is annihilated.

Our results are in part consistent with the work by Yermakova and Pertsov [18] who observed that the curvature of a circular spiral tip trajectory increased as the tip approached the boundary. The immediate consequence of the interaction between a tip trajectory and a boundary is an increase in the curvature in the tip trajectory. When the increase of the curvature of a tip trajectory near the boundary is insufficient to change its direction, then annihilation is obtained.

VII. RATIONALIZATION OF THE FRACTION OF TRAJECTORIES ANNIHILATED, $F_A(\theta_i)$, FIG. 7

Figure 7 shows the variation of the fraction of trajectories annihilated versus the incident angle θ_i. For each value of θ_i, a set of spirals are prepared for different values of $t_g \in [t_g^1, t_g^2]$ as discussed in connection with Figs. 5 and 6. These spiral waves for fixed θ_i hit the boundary with a unit of trajectory oriented in a way that depends on t_g. Some hit the boundary with a petal and others with an arc. The fraction of each kind of collision in the ensemble with $t_g \in [t_g^1, t_g^2]$ depends on θ_i. It was shown in the previous section that annihilation was due to the incomplete recovery of the j variable in regions where the front has to propagate in order to stay inside the domain as shown in Fig. 10. From this observation, we suggest that when annihilation occurs, the intersection of the tip trajectory with the boundary takes place at an arc of a unit of a spiral. This is anticipated, as the propagating region near the tip is less recovered when the tip is located at an arc as shown in Fig. 4(A).

In Fig. 11(A), we show the features of the tip trajectory at the boundary for a set of spirals for different θ_i that hit the boundary with an arc and get annihilated. This behavior is compared with the tip trajectories that get reflected as shown in Fig. 11(B). In this case, the trajectories hit the boundary with an arc, such as for $\theta_i=140°$ or with a petal as for $\theta_i=70°$ and $\theta_i=80°$. For some other angles such as $\theta_i=110°$ the orientation of the unit of trajectory is ambiguous. From Fig. 11(B), it is clear that interaction with an arc does not imply annihilation. For $\theta_i=140°$ in Fig. 11(A), the tip hits the boundary with a very early stage of an arc (shown in bold) giving annihilation. For the same angle in Fig. 11(B), the tip

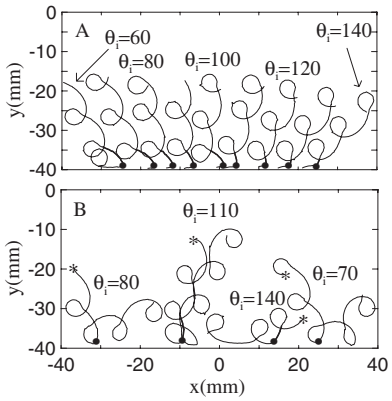

FIG. 11. Particular examples of trajectories of spirals that (A) annihilate at the boundary and (B) are reflected at the boundary.

hits the boundary when it is located at a later stage in the arc (shown in bold), giving reflection. Presumably, the excitability for this trajectory is just sufficient for the spiral to propagate, as illustrated in Fig. 4(A). This is consistent with the studies done by Efimov *et al.* [5] where they show that the threshold of excitation takes its largest value at the beginning of an arc and gradually decreases until it reaches a minimum value at a petal, increasing the chance of excitation. Boundary effects at later stages of the arc of a unit of trajectory are more effective at deforming the tip trajectory than at the beginning of the arc with low excitability.

We divide the variation of $F_A(\theta_i)$ versus θ_i in Fig. 7 into four intervals: (i) $\theta_i < 50°$ and $F_A(\theta_i)=0$; (ii) $\theta_i \in (50°, 120°]$ with $F_A(\theta_i)$ increasing to a maximum at $\theta_i = 120°$; (iii) $\theta_i \in (120°, 150°]$ with $F_A(\theta_i)$ decreasing to zero; and (iv) $\theta_i > 150°$ with $F_A(\theta_i) = 0$. When $\theta_i < 50°$, the spiral tip generally hits the boundary with a petal portion or with a very late stage of the arc portion of the spiral unit of trajectory and no annihilation occurs. A representative example is given by the trajectory with $\theta_i = 40°$ in Fig. 11(B). In this case, θ_i and the length of the arc are small enough, such that it is not possible to touch the boundary with an arc as a petal is suddenly formed and interaction takes place only with a petal. When the tip hits the boundary with a petal, reflection of the tip is observed as discussed in Sec. VI for Fig. 9.

For $\theta_i \in (50°, 120°]$, the probability that the spiral is annihilated at the boundary increases as θ_i increases. For $\theta_i \geq 50°$, the tip hits the boundary with the later stages of an arc and not with an early part, due to the orientation of the petals which face the boundary as shown in Fig. 11(A). Thus, in this case it is not possible to get an interaction of the tip trajectory with the boundary with an early portion of an arc. For $\theta_i \leq 120°$, the tip can hit the boundary with an early or a later arc portion of a spiral unit. Thus, there is a higher probability for the tip to hit the boundary, when the tip is located at an arc, for $\theta_i \leq 120°$ compared to $\theta_i \geq 50°$. Because the probability of annihilation increases when the tip is located at an arc, it gives the increasing dependence of $F_A(\theta_i)$ on θ_i for $\theta_i \in [50°, 120°]$ in Fig. 7.

It is useful to compare the results in Fig. 9 with the results discussed earlier in Fig. 5, also for $\theta_i = 120°$. Here, annihilation of the spiral wave occurs regardless of the portion of the arc that hits the boundary. In Fig. 5(A), annihilation of the spiral occurs because the two trajectories hit the boundary at early stages of an arc, when j is less recovered [Fig. 4(A)]. Although the curvature of the trajectory increases near the boundary, the deformation of the tip trajectory is insufficient to cause reflection of the spiral. In Fig. 5(B) with $t_g = 122$ ms, the trajectory moves to the left almost parallel to the boundary owing to the presence of the boundary, and the medium ahead of the wave can be activated and a petal is formed. At the end of the petal [end of the bold line in Fig. 5(B)], the region where the front needs to propagate to remain inside the domain is now at its maximum level of refractoriness [Fig. 4(A)] as a new petal has just formed leading to the annihilation of the spiral. The same explanation applies for $t_g = 129$ and 136 ms shown in Figs. 5(C) and 5(D), respectively.

Although both trajectories annihilate, the trajectory for $t_g = 122$ ms has an extra petal when compared with the one for $t_g = 105$ ms. A trajectory exists for $t_g \in [105°, 122°]$ such that the tip trajectory drifts parallel to the lower boundary. In this case, the spiral degenerates into a wave break propagating parallel to the boundary. For $t_g \in (120°, 150°)$, $F_A(\theta_i)$ is decreasing in θ_i. In this case, the interaction between the tip trajectory and the boundary takes place with an arc only.

As discussed at the end of the previous section and from [18], the effects of the boundary on a tip trajectory are reflected in an increase in the curvature of a tip trajectory. The reflection observed for $\theta_i = 140°$ in Fig. 11(B) shows that the interaction of the tip and the boundary occurs when the tip is at a later stage of a petal which is associated with a more excitable medium as illustrated in Fig. 4(A). The increase in curvature of the tip trajectory is enough to change the direction of the trajectory avoiding annihilation. For the annihilation observed for $\theta_i = 140°$ in Fig. 11(A), the interaction between the tip trajectory and the boundary occurs at an earlier stage of the petal than in the case where reflection is observed. In this case, the medium is less excitable than in the case of reflection for this same angle. Here, there is also an increase in the curvature of the tip trajectory due to boundary effects. However, in this case the change of curvature was less effective as the propagating region was less excitable than for the reflection case. Therefore, annihilation is obtained. It is clear that when θ_i is increased the supplementary angle $\theta_s = 180° - \theta_i$ is reduced. As θ_s gets smaller, the increase of curvature on the tip trajectory due to the presence of the boundary facilitates more the effect of reflection. This is due to the fact that for smaller θ_s a smaller change of direction of the tip trajectory is needed to keep the trajectory inside the domain. Therefore, $F_A(\theta_i)$ is decreasing in $\theta_i \in [120,150]$. The increase in curvature of the tip trajectory near the boundary is not as effective as for $\theta_i \in [50°, 120°]$. In this case, the incident angle θ_i is small enough such that in order to keep the trajectory inside the domain it is necessary to have a very strong change in the direction of the tip trajectory.

Finally, when $\theta_i > 150°$, the supplementary angle θ_s is too small and the increase of the curvature of the tip trajectory near the boundary is enough to redirect the spiral so that reflection occurs and $F_A(\theta_i)=0$. In this case, all the interactions between the tip trajectory and the boundary occur with an arc for which the excitability is low and there is no annihilation.

A. Reflection of spiral waves in the Fitzhugh-Nagumo model

It is of considerable interest to compare the results for the BR model with analogous results for the Fitzhugh-Nagumo model. The interaction of the spiral tip with a boundary on the square domain $[-10,10]\times[-10,10]$ was considered with the FHN model [11]

$$\frac{\partial u}{\partial t} = \frac{\partial^2 u}{\partial x^2} + \frac{\partial^2 u}{\partial y^2} + \frac{1}{\epsilon} u(1-u)\left(u - \frac{v+b}{a}\right),$$

$$\frac{\partial v}{\partial t} = u - v, \tag{3}$$

where $a=0.63$, $b=0.05$, and $\epsilon=0.02$ such that spiral waves in the R_∞ limit are generated. Examples of tip trajectories are

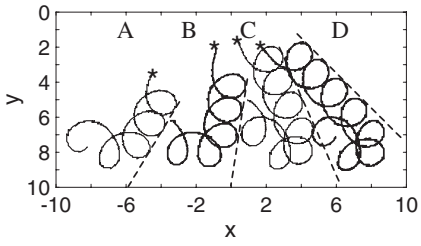

FIG. 12. Spiral tip trajectories for the FHN model given by Eq. (3) with $a=0.63$, $b=0.05$, and $\epsilon=0.02$. The incident angle is equal to (A) 118°, (B) 100°, (C) 68°, and (D) 45°. For all the incident angles θ_i considered, only reflection was observed; x and y are in mm.

shown in Fig. 12, where the tip trajectories with the incident angles $\theta_i=118°$, 199°, 68°, and 45° are shown. A large number of trajectories were considered for each angle and only reflection at the boundary was observed. This is because the recovery process for the FHN model is relatively faster than in the BR model, reflected by the fact that the ratio of the lengths of arc to petal portions of a unit of trajectory is smaller for the FHN model than for the BR model. Thus the difference in the behavior is due to the higher levels of excitability for the FHN model in the region where the tip of the spiral propagates.

The variable v in the FHN model is the recovery variable and plays a role analogous to j in the BR model. The value of v in the region ahead of the propagating front near the tip is in the interval $v \in [0.02, 0.05]$ while the tip traces a petal. The spiral wave in this instance propagates into a region of high excitability except at the beginning of an arc. For $v \in [0.05, 0.1]$, which corresponds to a lower excitability, the tip is located on the last part of the petal or for an arc. The value of $v \in [0.05, 0.1]$ lasts a very short time, giving a short length of the arc. Therefore, the probability of the interaction between the spiral and the boundary when the tip is located at an arc is small due to the fast recovery of the v variable. Thus, the probability of hitting the boundary with a petal for the FHN model is very high. Boundary effects in all cases for the FHN model deviate the spiral wave and reflection is observed.

VIII. SUMMARY

In this work, the phenomenon of annihilation and reflection of a spiral wave at a boundary for the Beeler-Reuter model, was considered. The R_∞ limit for which the petals of the tip trajectory lie on a straight line was studied numerically in detail. The results obtained with the R_∞ limit can provide an understanding of annihilation and reflection when R is finite.

We have shown that annihilation of the spiral depends strongly on the angle of incidence θ_i with respect to the boundary. The fraction of spirals that are annihilated for a given angle shown in Fig. 7 is one of the main results of this work. We have interpreted the results in Fig. 7 with an analysis based on the recovery gate j. This variable is responsible for the local reactivation of the Na channels and a lack of recovery will forbid the activation of an AP at such location. We have discussed how the different angles of incidence of the spiral tip trajectories affect the way the tip interacts with a boundary.

The analysis presented in this work bridges a couple of observations about simple rotation. For simple rotation, the spiral wave annihilates when the tip hits the boundary as shown by Krinsky *et al.* [40]. However, the studies presented by Yermakova and Pertsov [18] show that if the circular trajectory is close enough to the boundary an increase in the curvature is observed. From the studies presented in this paper, the results in [40,18] correspond to annihilation and reflection of the wave, respectively, with the corresponding arguments as discussed in Sec. VI. The present study suggests that simulations with other ionic models would be of considerable interest so that some general physical principles on annihilation and reflection might be deduced.

The dynamics of the j variable near the boundary shown in this paper play a very important role when a spiral wave interacts with an anatomic obstacle [9,29]. It has been observed from the numerical simulations that a spiral wave in the presence of an obstacle of some minimum size anchors to the obstacle [9,29]. In the same way, it has been observed that annihilation of a spiral wave occurs at a boundary of isolated tissue [9]. The results presented in this work extend these ideas to the possibility of the avoidance of attachment of the spiral to an obstacle and the annihilation of the spiral at the boundary.

ACKNOWLEDGMENTS

This research was supported in part by a grant to one of the authors (B.D.S.) from the Natural and Engineering Research Council of Canada. The other author (D.O.) was supported by the Mexican Consejo Nacional de Ciencia y Tecnologia (CONACYT). Support from the France Canada Research Fund (FCRF) is also acknowledged. We are grateful to Eric Cytrynbaum, Valentin Krinsky, and Alain Pumir for several useful discussions.

APPENDIX A: BEELER-REUTER EQUATIONS

The I_{ion} currents in Eq. (2) satisfy

$$I_{k_1} = 1.4\left[\frac{\exp[0.04(V+85)]-1}{\exp[0.08(V+53)]+\exp[0.04(V+53)]}\right] + 0.07\left[\frac{V+23}{1-\exp[-0.04(V+23)]}\right], \tag{A1}$$

$$I_{x_1} = 0.8x_1\left[\frac{\exp[0.04(V+77)]-1}{\exp[0.04(V+35)]}\right], \tag{A2}$$

$$I_{\mathrm{Na}} = (g_{\mathrm{Na}}m^3hj + g_{\mathrm{NaC}})(V - E_{\mathrm{Na}}), \tag{A3}$$

$$I_{\mathrm{Ca}} = g_s f d(V + 82.3 + 13.0287 \ln[\mathrm{Ca}^{2+}]), \tag{A4}$$

where $g_{\mathrm{Na}}=4$ mS cm^{-2}, $g_{\mathrm{NaC}}=0.003$ mS cm^{-2}, $E_{\mathrm{Na}}=50$ mV, and $g_s=0.09$ mS cm^{-2}. In this case, the ionic calcium

concentration $[Ca^{2+}]$ in the cytosol [Eq. (A4)] satisfies

$$\frac{d[Ca^{2+}]}{dt} = -10^{-7} I_{Ca} + 0.07(10^{-7} - [Ca^{2+}]). \quad \text{(A5)}$$

The variables x_1, m, n, j, d, and f are called gating variables and they are voltage and time dependent. They take values between zero and one. Each gating variable satisfies an ODE of the form

$$\frac{dX}{dt} = \frac{X_\infty - X}{\tau_X}, \quad \text{(A6)}$$

where $X=x_1$, m, n, j, d, and f. X_∞ and τ_X are given by

$$X_\infty = \frac{\alpha_X}{\alpha_X + \beta_X}, \quad \tau_X = \frac{1}{\alpha_X + \beta_X}, \quad \text{(A7)}$$

where

$$\alpha_X, \beta_X = \frac{C_X^1 e^{C_X^2(V+C_X^3)} + C_X^4(V + C_X^5)}{e^{C_X^6(V+C_X^3)} + C_X^7}, \quad \text{(A8)}$$

and the constants C_X^i, $i=1,7$, can be found in [5].

APPENDIX B: INITIAL CONDITIONS USED TO GENERATE SPIRAL WAVES

To generate an initial condition, the variables in the BR model took initially the values given by the steady state in the standard BR equations with the original parameters [5], i.e., $x_1=0.0056$, $m=0.011$, $h=0.99$, $j=0.97$, $d=0.003$, $f=1$, and $[Ca]=1\times10^{-7}$. A propagating front in the positive x direction that evolves into a spiral wave is generated by applying for the first millisecond a stimulus current of the form

$$I_{app}(x,y) = \begin{cases} 80\{(1+\exp[2.5(|x+\alpha y| - c_1)])\}^{-2} \\ -\ \{1+\exp[2.5(|x+\alpha y| - c_2)]\}^{-2}], & x \le 0 \\ 0, & x > 0, \end{cases} \quad \text{(B1)}$$

with $c_1=30$ and $c_2=25$. We choose in the first instance $\alpha=0$, so there is no y dependence in Eq. (B1). The shape of I_{app} vs x for these parameters is almost a square pulse with a width defined by the two roots of $I_{app}=0.5$, at $x_1=-22$ and $x_2=-30.5$ as shown by the horizontal parallel lines in Fig. 13(A). We integrate Eqs. (2), (A5), and (A6) to time $t_g=100$ ms and the AP propagates in the positive x direction. For a subsequent time equal to $\Delta t_g=20$ ms, the conductances g_{Na} and g_S are taken to be zero over the region $\alpha x > y - y_0$ delimited by the line $y=-20$. Thus, at time $t=t_g+\Delta t_g=120$ ms the pulse is as shown by the shaded region bounded by $y=-20$, where the conductances g_{Na} and g_S are restored to their original values. The result is a localized front with a free end propagating in the positive x direction, where this propagating front evolves into a spiral wave.

For the R_∞ case, we generate a spiral solution with a tip trajectory that has an incident angle θ_i, as discussed in the previous paragraph with $g_{Na}=2.37$ mS cm^{-2}, $g_S=0.003$ mS cm^{-2}, and $N=542$ points in each dimension. It turns out that the angle of incidence obtained for this spiral is $\theta_i=63°$, and the trajectory of the tip of the spiral is shown in Fig. 13(A). The formation of the spiral wave it follows from the propagation of this wave break and the excitability of the medium.

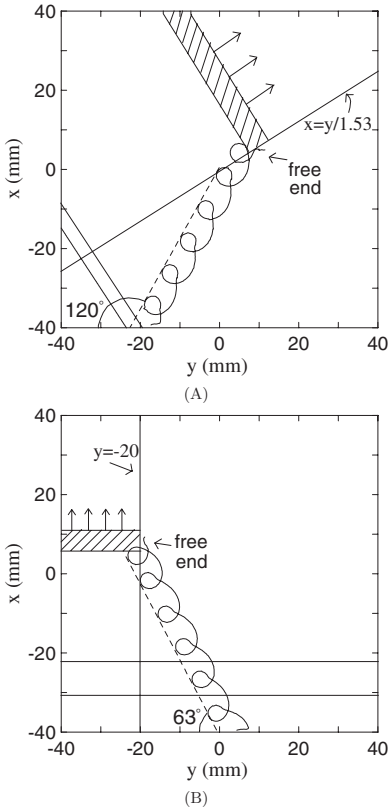

FIG. 13. Scheme used to generate a tip trajectory with incident angle (A) $\theta_i=63°$, and (B) $\theta_i=120°$. See the text for details.

Spiral tip trajectories with incident angle θ_i

In order to construct spirals such that their trajectories hit the boundary with a particular incident angle $\theta_i \neq 63°$, it is necessary to rotate I_{app} and $y > y_0$ in the (x,y) plane, and modify c_1, c_2, y_0, and t_g, depending on θ_i. Rotation of I_{app} for a particular θ_i is obtained by taking $\alpha=\tan(\frac{\theta_i-63°}{180°}\pi)$ in Eq. (B1). Thus for $\theta_i=120°$, $\alpha=1.53$ and $I_{app}=0.5$ gives the linear relationship between x and y as shown by the parallel lines at the left lower corner of Fig. 13(B). The values of c_1, c_2, y_0, and t_g are chosen by trial and error, in order to get a trajectory to hit the lower boundary. Once the values of c_1, c_2, y_0, and t_g are found for each angle, we change only one of the two parameters, t_g or y_0, in order to generate all the trajectories for that specific angle. For $\theta_i=120°$, $c_1=75$, $c_2=72$, $y_0=0$ mm, and $t_g=150$ ms. The conductances are taken as zero at the region $x > \frac{y}{1.53}$. A front with a free end (shaded region) evolves into a spiral that hits the lower boundary with a tip trajectory having $\theta_i=120°$.

[1] F. Fenton, E. Cherry, H. M. Hastings, and S. J. Evans, Chaos **12**, 852 (2002).
[2] R. A. Gray and J. Jalife, Chaos **8**, 65 (1998).
[3] J. Tyson, Lect. Notes Biomath. **100**, 569 (1994).
[4] A. T. Winfree, Chaos **8**, 1 (1998).
[5] I. R. Efimov, V. I. Krinsky, and J. Jalife, Chaos, Solitons Fractals **5**, 513 (1995).
[6] A. T. Winfree, J. Theor. Biol. **138**, 353 (1989).
[7] A. T. Winfree, Chaos **1**, 303 (1991).
[8] J. Davidenko, A. V. Pertsov, R. Salomonsz, W. Baxter, and J. Jalife, Nature (London) **355**, 349 (1992).
[9] A. M. Pertsov, J. M. Davidenko, R. Salomonsz, W. T. Baxter, and J. Jalife, Circ. Res. **72**, 631 (1993).
[10] P. Comtois, J. Kneller, and S. Nattel, Europace **7**, S10 (2005).
[11] D. Barkley, *Spiral Meandering, Chemical and Wave Patterns* (Kluwer, Netherlands, 1995).
[12] A. Karma, Phys. Rev. Lett. **65**, 2824 (1990).
[13] A. T. Winfree, *When Time Breaks Down* (Princeton University Press, Princeton, 1987), pp. 181–183.
[14] J. Beaumont, N. Davidenko, J. M. Davidenko, and J. Jalife, Biophys. J. **75**, 1 (1998).
[15] G. V. Osipov, B. V. Shulgin, and J. J. Collins, Phys. Rev. E **58**, 6955 (1998).
[16] F. Xie, Z. Qu, J. Weiss, and A. Garfinkel, Phys. Rev. E **59**, 2203 (1999).
[17] M. Gómez-Gesteira, A. P. Muñuzuri, V. Perez-Muñuzuri, and V. Perez-Villar, Phys. Rev. E **53**, 5480 (1996).
[18] Ye. A. Yermakova and A. M. Pertsov, Biophysics (Engl. Transl.) **31**, 932 (1986).
[19] E. V. Nikolaev, V. N. Biktashev, and A. V. Holden, Chaos, Solitons Fractals **9**, 363 (1998).
[20] I. Aranson, D. Kessler, and I. Mitkov, Physica D **85**, 142 (1995).
[21] G. W. Beeler and H. Reuter, J. Physiol. (London) **268**, 177 (1977).
[22] S. Bauer, G. Roder, and M. Bar, Chaos **17**, 015104 (2007).
[23] W. Chen, M. Potse, and A. Vinet, Phys. Rev. E **76**, 021928 (2007).
[24] P. Comtois and A. Vinet, Phys. Rev. E **72**, 051927 (2005).
[25] S. Dokos and N. H. Lovell, Prog. Biophys. Mol. Biol. **85**, 407 (2004).
[26] A. G. Kleber and Y. Rudy, Physiol. Rev. **84**, 431 (2004).
[27] J. P. Keener and J. Sneyd, *Mathematical Physiology, Interdisciplinary Applied Mathematics* (Springer, New York, 1998).
[28] T. Ikeda, T. Uchida, D. Hough, J. J. Lee, M. C. Fishbein, W. J. Mandel, P. S. Chen, and S. Karagueuzian, Circulation **94**, 1962 (1996).
[29] T. Ikeda, M. Yashima, T. Uchida, D. Hough, M. C. Fishbein, W. J. Mandel, P. S. Chen, and H. Karagueuzian, Circ. Res. **81**, 753 (1997).
[30] V. N. Biktashev, *Computational Biology of the Heart* (John Wiley & Sons, Chichester, 1997).
[31] L. Edelstein-Keshet, *Mathematical Models in Biology, Classics in Applied Mathematics* (SIAM, New York, 1988).
[32] R. Fitzhugh, Biophys. J. **1**, 445 (1961).
[33] F. Fenton, E. M. Cherry, A. Karma, and W. J. Rappel, Chaos **15**, 013502 (2005).
[34] H. Yang and B. Shizgal, Comput. Methods Appl. Mech. Eng. **118**, 47 (1994).
[35] D. Olmos and B. Shizgal (to be published).
[36] S. Rush and H. Larsen, IEEE Trans. Biomed. Eng. **25**, 389 (1978).
[37] Z. Qu and A. Garfinkel, IEEE Trans. Biomed. Eng. **46**, 1116 (1999).
[38] J. A. Trangenstein and C. Kim, J. Comput. Phys. **196**, 645 (2004).
[39] D. Olmos and B. Shizgal, J. Comput. Appl. Math. **193**, 219 (2006).
[40] V. I. Krinsky, V. N. Viktashev, and A. M. Pertsov, Ann. N.Y. Acad. Sci. **591**, 232 (1990).
[41] L. Glass and M. E. Josephson, Phys. Rev. Lett. **75**, 2059 (1995).
[42] J. J. Tyson and J. P. Keener, Physica D **32**, 327 (1988).